Frontiers in Bioscience Landmark

Front. Biosci. (Landmark Ed) **2026**; 31(10): 55597
https://doi.org/10.31083/FBL55597

Original Research

Integrated Bioinformatic and Experimental Analyses Identify CNTN6 as a Tumor-Promoting Factor and Prognostic Biomarker in Hepatocellular Carcinoma

Ranzhiqiang Yang[1], Jianing Yi[1], Jiyuan Zhang[1], Yuhuai Peng[2], Wenjie Gao[1], Chunzhao Yu[1,*]

[1]Department of General Surgery, Sir Run Run Hospital of Nanjing Medical University, 211166 Nanjing, Jiangsu, China
[2]Department of Hepatobiliary Surgery, Hunan Provincial People's Hospital/The First Affiliated Hospital of Hunan Normal University, 410005 Changsha, Hunan, China
*Correspondence: chunzhaoyu@hotmail.com (Chunzhao Yu)
Academic Editor: Sukmook Lee
Submitted: 4 July 2026 Revised: 6 September 2026 Accepted: 15 September 2026 Published: 23 October 2026

Abstract

Background: Hepatocellular carcinoma (HCC) remains a highly lethal malignancy, and reliable biomarkers are needed for prognostic stratification and the development of therapeutic strategies. Contactin-6 (CNTN6), a member of the immunoglobulin superfamily of cell-adhesion molecules, has not been fully characterized in HCC. **Methods:** Public datasets were used to evaluate *CNTN6* expression, clinicopathological associations, immune-cell infiltration, prognostic value, and correlations with drug sensitivity in HCC. The biological functions of *CNTN6* were assessed using HCC cell lines and xenograft models with *CNTN6* knockdown and overexpression. **Results:** *CNTN6* was upregulated in HCC tissues and was associated with several clinicopathological features. Elevated *CNTN6* expression was associated with poor survival outcomes and an M2-like macrophage infiltration signature. Functional enrichment analysis suggested that *CNTN6*-related proteins may participate in cell migration and oncogenic signaling pathways. *In vitro*, *CNTN6* knockdown suppressed HCC cell proliferation, colony formation, migration, and invasion, whereas *CNTN6* overexpression enhanced these malignant phenotypes. *In vivo*, *CNTN6* knockdown reduced xenograft tumor growth and altered CD86/CD206 immunostaining patterns. **Conclusions:** *CNTN6* is upregulated in HCC and may function as a tumor-promoting factor associated with poor prognosis and macrophage-related immune remodeling. Further mechanistic and clinical validation is warranted.

Keywords: hepatocellular carcinoma; CNTN6; M2 macrophage; tumor immunity

1. Introduction

Despite advances in surveillance, local therapy, targeted therapy, and immunotherapy, the prognosis of advanced hepatocellular carcinoma (HCC) patients remains unsatisfactory because of late diagnosis, intra-tumoral heterogeneity, and therapeutic resistance [1,2,3,4]. Although diagnostic and therapeutic strategies for HCC patients have improved, its pathogenesis remains complex, involving genetic alterations, epigenetic dysregulation, chronic inflammation, and tumor-microenvironment remodeling [5,6]. These factors contribute to marked disease heterogeneity, aggressive biological behavior, and frequent resistance to existing therapies [7]. Thus, a systematic elucidation of the fundamental molecular drivers governing hepatocarcinogenesis and disease advancement remains imperative [8]. Meanwhile, identifying and validating novel diagnostic biomarkers and therapeutic targets are vital to the optimization of long-term survival outcomes in HCC patients.

Cell adhesion molecules contribute to tumor initiation and progression by regulating cell-cell interactions, extracellular matrix adhesion, cell migration and invasion, and immune-cell communication [9,10,11]. CNTN6, also termed contactin-6, is a glycosylphosphatidylinositol-anchored glycoprotein classified in the contactin subdivision of immunoglobulin superfamily cell adhesion molecules [12]. CNTN6 is involved in nervous-system development, particularly neuronal connectivity, axon guidance, and synaptic organization [13]. Previous studies have linked CNTN6 dysregulation to neurodevelopmental and neurological disorders; however, its role outside the nervous system remains incompletely characterized [14]. Remarkably, an increasing body of evidence suggests that CNTN6 may also demonstrate significant pathophysiological significance in non-neural tissues, especially in various solid tumors. Emerging evidence suggests that CNTN-family molecules may exert biological roles beyond the nervous system, including potential involvement in tumor progression [15].

However, the expression features, prognostic value, and biological mechanisms involving *CNTN6* in HCC still lack comprehensive investigation. HCC develops in a distinctive inflammatory and fibrotic hepatic microenvironment, where neoplastic cells maintain intimate communication with stromal cells, immune subsets, and complex

Copyright: © 2026 The Author(s). Published by IMR Press.
This is an open access article under the CC BY 4.0 license.

Publisher's Note: IMR Press stays neutral with regard to jurisdictional claims in published maps and institutional affiliations.

cytokine networks [16,17,18,19]. Whether *CNTN6* acts as a tumor-promoting factor or suppressive regulator in HCC requires systematic investigation. Furthermore, the correlation between *CNTN6* expression levels and clinicopathological characteristics (i.e., tumor stage, histological grade, vascular invasion, and metastatic potential), as well as prognostic outcomes in HCC patients, requires systematic investigation. Clarifying these mechanistic questions is paramount to deciphering *CNTN6*'s pathobiological contributions to HCC and its potential therapeutic applications. In the present study, we combined bioinformatic mining from public datasets with cell- and animal-based assays to characterize the expression profile, prognostic significance, and biological functions of *CNTN6* in HCC. By analyzing public datasets and publicly available protein-expression evidence, we evaluated *CNTN6* expression in liver hepatocellular carcinoma (LIHC) tumor tissues and paired peritumoral tissues and analyzed potential correlations of its expression level with clinicopathological features as well as patient prognosis. Furthermore, we used *CNTN6*-knockdown HCC cell models and a xenograft tumor model to investigate its effects on cell proliferation, colony formation, cell migration and invasion, and tumor growth, and explored *CNTN6*-associated functional networks through enrichment analyses. This study elucidates *CNTN6*'s functional role in LIHC pathogenesis, offering novel insights into hepatocarcinogenesis while assessing its potential as a diagnostic biomarker or therapeutic target [20,21].

2. Materials and Methods

2.1 Public Data Acquisition and Survival Analysis

We collected clinical information and RNA sequencing (RNA-seq) raw data belonging to The Cancer Genome Atlas (TCGA)-LIHC patient cohort from the official TCGA repository. Meanwhile, transcriptomic profiles derived from intact, non-diseased liver tissue samples were acquired through the GTEx platform [22,23]. Publicly available datasets deposited with the Human Protein Atlas (HPA) were applied to profile the protein expression signatures of CNTN6 across liver tissues [24]. Expression values were transformed to TPM values before between-group comparisons, and batch effects between the TCGA-LIHC and GTEx datasets were corrected using the ComBat algorithm implemented in the R package "sva". Clinicopathological variables, including age, sex, pathologic stage, histologic grade, vascular invasion, AFP and albumin levels, and tumor status, were extracted from TCGA-LIHC when available. Variables with excessive missing values were excluded from regression analyses. We partitioned LIHC participants into high- and low-expression CNTN6 cohorts based on the median cutoff of *CNTN6* mRNA transcript abundance. Kaplan-Meier survival curves were generated using the R "survival" package, where inter-group survival discrepancies were evaluated using the log-rank statistical test. Univariate and multivariate Cox regression models were constructed to probe the independent prognostic predictive capacity of CNTN6 within the LIHC population.

2.2 Immune-Cell Infiltration Analysis

Immune-cell infiltration profiles in tumor specimens were quantified using CIBERSORT with the standard LM22 signature matrix [25]. Deconvolution was performed with 1000 permutations, and Specimens passing the CIBERSORT threshold ($p < 0.05$) were retained for follow-up analyses to ensure data credibility. The algorithm computed relative fractions of 22 discrete immune-cell subsets in tumor tissues. Spearman correlation tests were then conducted to examine how CNTN6 expression was correlated with the extent of immune-cell infiltration.

2.3 Functional Enrichment Analysis

We performed Spearman correlation tests to filter genes strongly associated with CNTN6 expression across TCGA-LIHC samples. Transcripts with ($|r| > 0.3$) and adjusted $p < 0.05$ were imported into the R clusterProfiler package for Gene Ontology (GO) functional annotation and Kyoto Encyclopedia of Genes and Genomes (KEGG) pathway enrichment [26]. Enrichment results were plotted using ggplot2, and inter-gene interaction maps were built based on data retrieved from STRING and GeneMANIA platforms [27,28]. Independent prognostic factors derived from multivariate Cox regression were utilized to construct a survival nomogram. Calibration curves were generated to assess the degree of agreement between predicted and real 1-, 3-, and 5-year overall survival rates.

2.4 Drug Sensitivity Analysis

We performed drug susceptibility evaluation via the Gene Set Cancer Analysis (GSCA) online platform, relying on aggregated drug response datasets extracted from the Cancer Therapeutics Response Portal (CTRP). Spearman rank correlation coefficients were computed to measure the potential association between *CNTN6* transcript abundance and drug susceptibility metrics, and the resulting correlation patterns were correspondingly visualized. All screened candidate chemical agents merely served as materials for hypothesis generation.

2.5 Tissue Microarray (TMA)

TMA samples were purchased from the Central Laboratory of Hunan Provincial People's Hospital. The TMA dataset included 100 cases (8 cases were excluded from the analysis due to tissue loss) of HCC tumors and matched adjacent tissues. It also includes clinical and prognostic information. The TMA approval process was reviewed by the Medical Ethics Committee of Hunan Provincial People's Hospital/The First Affiliated Hospital (IRB Approval No.: 2024-302).

IHC staining was performed using the standard EnVision protocol. Briefly, slides underwent deparaffinization, antigen retrieval in 10 mM citrate buffer (pH 6.0, 121 °C, 3 min), endogenous peroxidase blocking and serum blocking. Slides were incubated with anti-CNTN6 primary antibody (1:400, Cat#A14275, ABclonal Biotechnology Co., Ltd., Wuhan, Hubei, China, 1:400) overnight at 4 °C, followed by HRP-conjugated secondary antibody (1:200, Cat#AS014, ABclonal Biotechnology Co., Ltd., Wuhan, Hubei, China, 1:200) and DAB visualization. Negative controls were set with PBS substituting the primary antibody. Two board-certified pathologists blinded to clinical data independently scored samples by multiplying staining intensity (0–3) and positive tumor cell percentage (0–4), yielding a final score of 0–12. Discrepant scores were resolved by a third senior pathologist. The median was used to determine the best cut-off value for high/low CNTN6 expression.

2.6 Cell Culture

We cultured a HCC cell line, MHCC-97Hsupplied by the Fudan Institute of Biomedical Sciences Cell Center (Shanghai, China), in standard high-glucose Dulbecco's Modified Eagle's Medium (DMEM). The complete medium contained 10% fetal bovine serum and 1% penicillin-streptomycin antibiotic mixture. Cells were incubated at 37 °C in a humidified incubator with a constant 5% CO_2 air supply. The HCC cell line was validated by Short Tandem Repeat (STR)-PCR profiling and confirmed as negative for mycoplasma infection. Parallel experiments in HepG2 cells produced comparable findings; however, given the controversial disease origin of HepG2 and its current classification in the Cellosaurus database (CVCL_0027) as not being a hepatocellular carcinoma cell line, these data were not included in the present manuscript.

2.7 Lentiviral Transduction and CNTN6 Knockdown

Lentiviral particles carrying short hairpin RNA (shRNA) targeting *CNTN6*: 5′-CCGGCCCTCCATTGAAGTGGTATTTCTCGAGAAATACCACTTCAATGGAGGGTTTTTG-3′, or a non-targeting control shRNA, were used to establish stable CNTN6-knockdown HCC cells. We transduced the two HCC cell lines with a lentivirus in the presence of polybrene, followed by antibiotic selection. Western blot (WB) assays were used to verify CNTN6 knockdown efficiency.

2.8 Lentiviral Transfection and Overexpression of CNTN6

To establish stable CNTN6-overexpressing HCC cell line, a lentiviral transfection system was applied in HCC cells. Briefly, the full-length human CNTN6 coding sequence (CDS, 3087 bp) of human CNTN6 was amplified from the canonical transcript NM_001289080.2, which encodes the 1028-amino-acid full-length CNTN6 protein, inserted into the lentiviral vector, and an empty vector was used as the negative control (Vector). HCC cells were seeded in complete culture medium and maintained to reach an appropriate confluence before lentiviral infection. Subsequently, lentivirus containing the CNTN6 overexpression sequence or an empty vector was added to the cell culture medium. After 12–14 h of incubation, the virus-containing medium was replaced with fresh complete medium. At 72 h post-infection, puromycin screening was performed to eliminate uninfected cells and obtain stably transfected cell line. The overexpression efficiency of CNTN6 at the protein level was further validated by Western blot assay.

2.9 WB Analysis

For Western blot (WB) analysis, HCC cells stably transfected with empty vector (Vector), CNTN6 overexpression (CNTN6-OE), shRNA negative control (shNC), and CNTN6 knockdown (*sh*CNTN6) constructs were cultured in 6-well plates to 70%–80% confluency. Cells were lysed in RIPA buffer containing protease inhibitors, and total protein concentrations were determined using a BCA protein assay kit (Cat#C0121, Baiqiandu, Wuhan, Hubei, China). Equal amounts of protein were resolved and electrotransferred onto PVDF membranes. After blocking, membranes were incubated with primary antibodies (Cat#A12289 and Cat#A14275, ABclonal Biotechnology Co., Ltd., Wuhan, Hubei, China) targeting proteins of interest and Tubulin, followed by HRP-conjugated secondary antibodies (AS070, ABclonal Biotechnology Co., Ltd., Wuhan, Hubei, China). Protein bands were visualized using ECL chemiluminescent substrate (Cat#C0330, Baiqiandu, Wuhan, Hubei, China) and imaged. Tubulin was applied as an internal reference for normalizing relative target protein expression.

2.10 Cell Viability Assay

Cell Counting Kit-8 (CCK-8) colorimetric assay was used to evaluate the proliferative ability of HCC cells. MHCC-97H cells stably transfected with empty vector (Vector), CNTN6 overexpression (CNTN6-OE), shRNA negative control (shNC), and CNTN6 knockdown (*sh*CNTN6) were seeded in 96-well plates at a density of 2000 cells per well. After the cells adhered to the plate, they were treated with MLN2238 (Cat#No. A4008, APExBIO, Shanghai, China), prepared according to the manufacturer's instructions. CCK-8 working solution (Cat#C0037, Beyotime, Beijing, China) was added at five indicated time points (0, 12, 24, 48, and 72 h), followed by a 2 h incubation at 37 °C. The optical absorbance at 450 nm was measured using a microplate spectrophotometer (ELx800, BioTek Instruments, Inc., Winooski, VT, USA). Cell-free blank wells were set for background signal correction, and all experiments were performed in triplicate.

2.11 Colony Formation Assay

Logarithmic-phase HCC cells were subjected to digestion with trypsin, plated at a density of 500 cells per well in six-well culture dishes, and incubated for 10–14 days at 37 °C in a 5% CO_2 air environment with regular medium replacement until macroscopic cell colonies emerged. Colonies were fixed in methanol for 15 min, stained using 0.1% crystal violet solution over a 10-minute period, and counted after repeated phosphate-buffered saline (PBS) rinses. Colonies were quantified using ImageJ software (v1.54, National Institutes of Health, Bethesda, MD, USA).

2.12 Flow Cytometry

Apoptotic rates were determined via the Annexin V-PE/7-AAD apoptosis detection kit (Cat#40310ES60, Yeasen Biotechnology Co., Ltd., Shanghai, China). After trypsin dissociation and rinsing, cell pellets were incubated with 5 μL PE-Annexin V and 10 μL 7-AAD for 15 min at room temperature in the dark.

Macrophage phenotypic polarization was evaluated via flow cytometry after non-contact co-culture. THP-1 (Cat#CL-0233, Procell, Wuhan, Hubei, China) monocytes were stimulated with phorbol 12-myristate 13-acetate (PMA) (Cat#16561-29-8, MedChemExpress, Shanghai, China) to differentiate into adherent macrophages. The resulting macrophages were co-cultured with control and CNTN6-overexpressing MHCC-97H HCC cells in a Transwell non-contact system, then collected and stained with fluorescence-conjugated anti-CD206 antibody (Cat#32221ES60, Yeasen Biotechnology Co., Ltd., Shanghai, China) for 15 min at room temperature in the dark.

All samples were quantified on a BD Accuri C6 flow cytometer with FACSuite software (BD Bioscience, Milpitas, CA, USA). Compensation was calibrated using single-stained controls, and the complete gating strategy is provided (**Supplementary Fig. 1J**). Briefly, cell debris was excluded by FSC-A vs SSC-A gating, and singlets were isolated via FSC-H vs FSC-A. For apoptosis analysis, four quadrants were defined: Annexin V^-7-AAD^- (viable), Annexin V^+7-AAD^- (early apoptosis), Annexin V^+7-AAD^+ (late apoptosis/necrosis), Annexin V^-7-AAD^+ (necrosis). For CD206 detection, the positive threshold was determined by matched isotype control. Unstained and isotype controls were included to confirm specificity.

2.13 Scratch-Wound-Healing Assay

The scratch-wound-healing assay was adopted to detect the migration ability of CNTN6-knockdown MHCC-97H cells. Stable CNTN6 knockdown and NC HCC cells were cultured to confluence in 6-well plates, then a consistent scratch was made across the cell monolayer with a pipette tip. After PBS rinsing to remove floating dislodged cells, culture medium without fetal bovine serum was used to refresh the cell medium. Images of the scratch wounds were captured under a microscope at 0 and 24 h. ImageJ software was employed to measure the extent of wound closure in order to calculate cell migration ratios, with three biological replicates for each group.

2.14 Transwell Cell Migration and Invasion Assay

Transwell inserts were adopted to evaluate the migratory and invasive capacity of HCC cells. Inserts for cell invasion assays were pre-coated with Matrigel as per the manufacturer's guidelines, whereas uncoated inserts were used for migration assays. HCC cells suspended in serum-free medium were seeded into the upper Transwell compartments, and medium supplemented with 10% fetal bovine serum (FBS) was loaded into the lower chambers as a chemoattractant. Following 24-h incubation, cells adhering to the basal membrane were fixed and stained with crystal violet, with cell numbers quantified across three randomly selected microscopic fields.

2.15 EdU Staining

HCC cells were seeded into six-well culture dishes and incubated overnight prior to experimental intervention. EdU working solution (Cat#C0078S, Beyotime, Beijing, China) was prepared and then added to wells after pre-warming, with the volume adjusted with culture medium. Following a 2-h incubation period, cells sequentially underwent fixation, rinsing with PBS, and membrane permeabilization. Subsequently, 0.5 mL of click reaction mixture was added per well for 30 mins and incubated in the dark at room temperature. After removal, cells were washed three times (3–5 mins each) with PBS before nuclear staining for fluorescence microscopy observations.

2.16 ELISA Analysis

HCC cells stably transfected with empty vector (Vector) and CNTN6 overexpression (CNTN6-OE) were used for co-culture experiments. THP-1 monocytes were induced to differentiate into macrophages via PMA stimulation. Subsequently, HCC cells from each group were co-cultured with differentiated macrophages using a Transwell non-contact co-culture system to simulate the tumor immune microenvironment. After sustained co-culture, cell culture supernatants were collected and centrifuged to remove cell debris. The concentrations of the immunosuppressive cytokines interleukin-10 (IL-10) and transforming growth factor-β (TGF-β) in the supernatants were quantitatively detected using corresponding commercial ELISA kits strictly according to the manufacturer's protocols. Specifically, Human TGF-β ELISA Kit (Cat#PT880, Beyotime Biotechnology, Shanghai, China) and Human IL-10 ELISA Kit (Cat#PI528, Beyotime Biotechnology, Shanghai, China) were used in this study. The optical density (OD) values of each well were measured at the corresponding wavelength with a microplate spectrophotometer (ELx800, BioTek Instruments, Inc., Winooski, VT, USA),

and standard curves were generated to calculate the relative cytokine levels in each group. All experiments were performed in triplicate biological replicates to guarantee the reliability and reproducibility of the results.

2.17 Animal Experiments

Six-week-old male BALB/c nude mice purchased from Jiangsu Jicui Biopharmaceutical were acclimated for 7 days under specific pathogen-free housing (22 °C–25 °C, 12-h light–dark cycle) with *ad libitum* access to standard chow and drinking water. Animals were randomly divided into shNC and *sh*CNTN6 cohorts (n = 5 per group) and subcutaneously injected with MHCC-97H cells stably carrying the corresponding shRNA constructs. Tumor dimensions were measured every 2 days starting from Day 8 post-inoculation, and tumor volume was calculated using the formula: $V = \text{length} \times \text{width}^2 / 2$.

For euthanasia of mice, USP Grade A cylinder-compressed CO_2 with a purity of ≥99% was used as the exclusive gas source, equipped with a precise flow rate regulation device. Euthanasia was conducted in a dedicated transparent 9-liter euthanasia chamber, which was not situated in the original animal housing room. For each batch of mice, adequate space was ensured in the chamber to allow free body posture adjustment.

The chamber was not pre-charged with CO_2 before the mice were placed inside. CO_2 was infused at a constant flow rate of 5.4 L/min to induce rapid loss of consciousness in mice. The respiratory status and ocular manifestations of each mouse were continuously observed. After respiratory arrest was confirmed in all mice, CO_2 infusion was maintained for at least 1 additional minute. Mice were removed from the chamber only after respiratory arrest and pupillary dilation were verified. Death was confirmed by the combined criteria of cardiac arrest and limb rigidity. If complete death was not confirmed, secondary euthanasia via cervical dislocation was performed immediately. After each batch of procedures, the chamber was thoroughly cleaned to eliminate animal pheromones before reuse.

All animal experiments and procedures followed the protocol of the Animal Ethics Institution of Hunan Provincial People's Hospital (Approval No. 2025062).

2.18 Histological Staining, Immunohistochemistry, and Immunofluorescence Assays

Formalin-fixed, paraffin-embedded xenograft tumor tissues were serially sectioned to 5 µm. After routine deparaffinization, alcohol-gradient rehydration, and antigen retrieval treatment, tissue slides were subjected to hematoxylin and eosin (H&E) staining for histomorphological observation. For Ki-67 immunohistochemistry (IHC), tissue slices were incubated with 3% H_2O_2 solution to eliminate endogenous peroxidase activity, followed by overnight incubation with primary anti-Ki-67 antibody (Cat#A20018, ABclonal Biotechnology Co., Ltd., Wuhan, Hubei, China, 1:3000) at 4 °C and subsequent secondary antibody incubation. Immunoreactive signals were visualized via 3,3′-diaminobenzidine (DAB) chromogenic substrate reaction, and hematoxylin counterstaining was conducted afterwards. All tissue images were acquired under an optical light microscope.

Terminal deoxynucleotidyl transferase-mediated dUTP nick end labeling (TUNEL) staining was carried out to detect apoptotic cells in xenograft tissue sections using the *In Situ* Cell Death Detection Kit, Fluorescein, strictly following the manufacturer's instructions. Cell nuclei were counterstained with 4′,6-diamidino-2-phenylindole (DAPI), and fluorescence signals were imaged with a laser scanning confocal microscope.

For double immunofluorescence (IF) labeling targeting CD86 and CD206, tissue sections were incubated with the two primary antibodies simultaneously at 4 °C overnight, prior to incubation with fluorophore-tagged secondary antibodies. DAPI was applied again for nuclear counterstaining, and all IF images were recorded via the same fluorescence microscope.

2.19 Statistics

Statistical analyses were performed using GraphPad Prism v.8.0 and R (ggplot2). The normality of continuous data was assessed using the Shapiro–Wilk test, and homogeneity of variances was evaluated using Levene's test. All data subjected to parametric tests met the assumptions of normal distribution and equal variance. Continuous data (means ± standard error of the mean [SEM]) were compared using Student's *t*-test. For survival analysis, patients were stratified into high- and low-*CNTN6* expression groups based on the median *CNTN6* mRNA expression level, and survival differences were assessed via the log-rank test. For multiple subgroup survival analyses, the Benjamini–Hochberg false discovery rate (FDR) correction was applied to adjust for multiple testing, and adjusted *p*-values < 0.05 were considered statistically significant. All *in vitro* functional experiments were performed with at least 3 independent biological replicates and 3 technical replicates per sample. *In vivo* xenograft experiments included 5 mice per group as biological replicates.

3. Results

3.1 CNTN6 Is Upregulated in HCC and Associated With Clinicopathological Features

We initially profiled mRNA transcript levels of *CNTN6* across a spectrum of human malignancies based on RNA-seq data retrieved from TCGA and GTEx repositories [29,30]. Within this tumor panel, *CNTN6* transcript levels were markedly elevated in multiple malignancies such as LIHC, whereas its abundance was diminished in lung adenocarcinoma and lung squamous cell carcinoma (Fig. 1A and **Supplementary Table 1**). After integrating normal hepatic tissue profiles derived from GTEx, *CNTN6* tran-

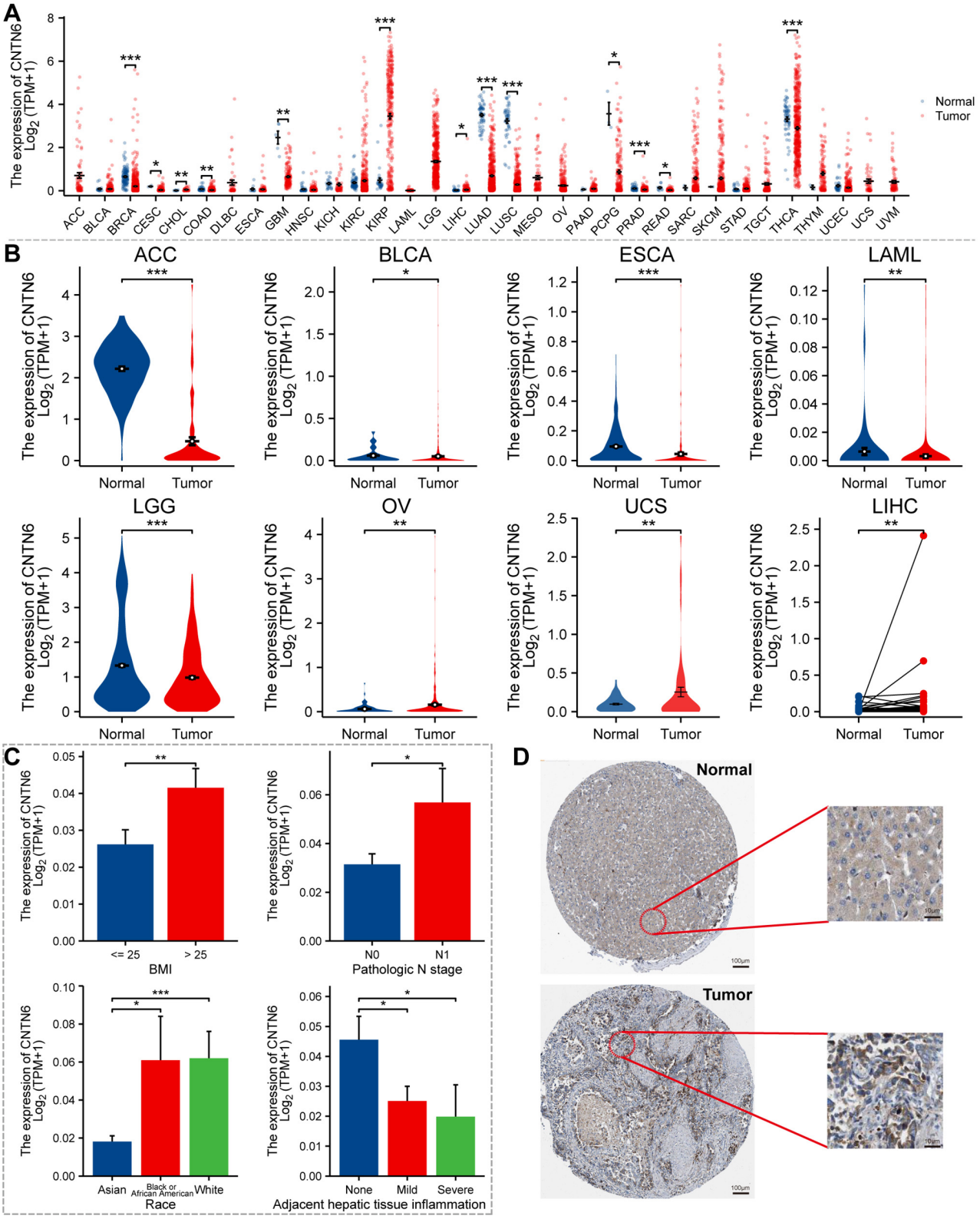


Fig. 1. Contactin-6 (CNTN6) expression across cancer types and its association with clinicopathological features in liver hepatocellular carcinoma (LIHC). (A) CNTN6 mRNA expression in pan-cancer. (B) CNTN6 expression in selected cancer types after inclusion of matched or GTEx-derived normal tissues. (C) The relationship between clinical characteristics such as Body Mass Index (BMI), pathologic N stage, ethnicity, tissue inflammation, and CNTN6 expression level. (D) Representative immunohistochemical staining results for CNTN6 in hepatocellular carcinoma (HCC) and adjacent non-tumor liver tissues. The bar in the main image represents 100 μm, and the bar in the 10x magnification image represents 10 μm. *$p < 0.05$; **$p < 0.01$; ***$p < 0.001$.

script abundance was confirmed to be markedly elevated in LIHC lesions relative to non-diseased liver parenchyma (Fig. 1B). In TCGA-LIHC, comparisons between high and low CNTN6 expression groups (Table 1) showed that CNTN6 expression was significantly associated with ethnicity and adjacent hepatic tissue inflammation status, but not with body mass index (BMI, $p = 0.213$) or pathologic lymph node (N) stage ($p = 0.098$). The continuous expression pattern of CNTN6 across clinical subgroups (Fig. 1C). Immunohistochemical data from the HPA revealed stronger CNTN6 staining in HCC tissues than in adjacent non-tumor tissues (Fig. 1D). These data suggest that *CNTN6* is upregulated in HCC and may be associated with HCC progression.

3.2 High CNTN6 Expression Is Associated With Unfavorable Survival Outcomes in HCC

To explore the relationship between CNTN6 and the clinical characteristic information of patients with liver tumors, we conducted a more in-depth analysis. Kaplan-Meier survival analysis showed that high CNTN6 expression was associated with shorter OS, progression-free interval (PFI), and disease-specific survival (DSS) in HCC patients (Fig. 2). Stratified survival analyses further suggested that the prognostic association of CNTN6 was evident in several clinical subgroups, including patients stratified by Weight >70 kg, Weight ≤70 kg, Age >60 years, Age ≤60 years, Male, Pathologic N stage: N0, Pathologic M stage: M0, Histologic grade: G2, Histological type: hepatocellular carcinoma, Prothrombin time: ≤4, Albumin (g/dL): ≥3.5, AFP (ng/mL): ≤400, Tumor status: tumor free, vascular invasion: Yes, Residual tumor: R0, Vascular invasion: No.

3.3 CNTN6 Expression Is Associated With Immune-Cell Infiltration and M2-Like Macrophage Signatures

Mounting evidence has confirmed that intratumoral immune-cell infiltration exerts profound impacts on HCC progression and patient clinical prognosis [31,32,33]. To dissect the regulatory link between CNTN6 and intratumoral immune-cell infiltration, we systematically assessed the correlation of CNTN6 expression levels with the abundance of immune-cell subsets across multiple tumor cohorts (Fig. 3A). This analysis revealed significant correlations between CNTN6 expression and tumor-infiltrating immune-cell populations, particularly B lymphocytes, T lymphocytes, and macrophages across multiple malignancies. In LIHC, CNTN6 expression was positively associated with M2 macrophage infiltration and negatively associated with M1 macrophage infiltration (Fig. 3B,C). The CNTN6-low cohort exhibited elevated M1 macrophage infiltration, while CNTN6-high tumors demonstrated predominant M2 polarization (Fig. 3B,C), suggesting an association between CNTN6 expression and a macrophage-related immunosuppressive signature in HCC [34,35,36]. Through further analysis, we found that CNTN6 expression was correlated with M2-macrophage-related markers, immunosuppression-associated molecules, and tumor-proliferation-related genes (Fig. 3D–F). Therefore, these results suggest that CNTN6 may be associated with malignant progression and immune remodeling in HCC [37] (**Supplementary Tables 2,3**). GO enrichment network analysis showed that CNTN6-related genes were mainly enriched in multiple biological function terms (Fig. 3G). The KEGG pathway enrichment network indicates that these genes are mainly involved in multiple signaling pathways related to cancer (Fig. 3H). At the DNA methylation level, we profiled 11 CpG loci spanning the CNTN6 promoter and gene body in TCGA-LIHC. All loci showed significant hypomethylation in HCC tissues, and this epigenetic feature was recapitulated in an independent GEO cohort (**Supplementary Fig. 1C–F**). We further screened for miRNAs mediating post-transcriptional regulation of CNTN6. Multidimensional cross-screening of TCGA-LIHC expression-correlation data prioritized a panel of macrophage-associated miRNA candidates, including miR-27a-3p, miR-424-5p, and miR-659-3p (**Supplementary Fig. 1G–I**).

3.4 Construction of a CNTN6-Related Prognostic Nomogram and Drug-Sensitivity Correlation Analysis

To explore the prognostic factors of HCC patients, Cox univariate and multivariate regression analyses were performed, and the results showed that tumor stage, tumor status, and CNTN6 expression level were the factors affecting the prognosis of HCC patients (**Supplementary Table 4**). To better predict the 1-, 3-, and 5-year survival probabilities of HCC patients, we developed a nomogram incorporating pathologic stage, tumor status, and CNTN6 expression [38] (Fig. 4A). Calibration curves showed acceptable agreement between nomogram-predicted and observed 1-, 3-, and 5-year OS probabilities (Fig. 4B). Subsequently, we conducted a drug sensitivity analysis of CNTN6 and CTRP [39,40]. The results showed that CNTN6 expression was negatively correlated with the AUC(Area Under the dose-response curve) of most chemotherapeutic and targeted agents, suggesting that elevated CNTN6 expression corresponds to higher drug sensitivity and better potential therapeutic response to these compounds, including BMS-345541, CR-1-31B, MLN2238, narciclasine, ouabain, parbendazole, and triazolothiadiazine (Fig. 4C and **Supplementary Table 5**) [41]. Furthermore, the inhibitory effect of MLN2238 on HCC cell viability was investigated, and the results showed that MLN2238 significantly inhibited tumor cell viability (**Supplementary Fig. 1K,L**).

3.5 Expression Characteristics and Prognostic Significance of CNTN6 in TMA

Given the exploratory nature of the subgroup analyses and the multiplicity of comparisons, some of the observed associations may be due to chance. We therefore used our

Table 1. Correlation between CNTN6 expression and clinicopathological features of LIHC cases.

Characteristics	Low expression of CNTN6	High expression of CNTN6	*p*-value
n	187	187	
Pathologic T stage, n (%)			0.040
T1	106 (28.6%)	77 (20.8%)	
T2	42 (11.3%)	53 (14.3%)	
T3	34 (9.2%)	46 (12.4%)	
T4	5 (1.3%)	8 (2.2%)	
Pathologic N stage, n (%)			0.098
N0	138 (53.5%)	116 (45%)	
N1	0 (0%)	4 (1.6%)	
Pathologic M stage, n (%)			0.678
M0	139 (51.1%)	129 (47.4%)	
M1	3 (1.1%)	1 (0.4%)	
Pathologic stage, n (%)			0.040
Stage I	100 (28.6%)	73 (20.9%)	
Stage II	40 (11.4%)	47 (13.4%)	
Stage III	34 (9.7%)	51 (14.6%)	
Stage IV	3 (0.9%)	2 (0.6%)	
Tumor status, n (%)			0.878
Tumor-free	100 (28.2%)	102 (28.7%)	
With tumor	77 (21.7%)	76 (21.4%)	
Gender, n (%)			0.224
Female	55 (14.7%)	66 (17.6%)	
Male	132 (35.3%)	121 (32.4%)	
Race, n (%)			<0.001
Asian	100 (27.6%)	60 (16.6%)	
Black or African American	6 (1.7%)	11 (3%)	
White	73 (20.2%)	112 (30.9%)	
Age (years), n (%)			0.719
≤60	90 (24.1%)	87 (23.3%)	
>60	96 (25.7%)	100 (26.8%)	
Weight (kg), n (%)			0.196
≤70	98 (28.3%)	86 (24.9%)	
>70	75 (21.7%)	87 (25.1%)	
Height (cm), n (%)			0.027
<170	112 (32.8%)	89 (26.1%)	
≥170	61 (17.9%)	79 (23.2%)	
BMI (kg/m^2), n (%)			0.213
≤25	95 (28.2%)	82 (24.3%)	
>25	75 (22.3%)	85 (25.2%)	
Residual tumor, n (%)			1
R0	163 (47.2%)	164 (47.5%)	
R1	8 (2.3%)	9 (2.6%)	
R2	1 (0.3%)	0 (0%)	
Histological type, n (%)			0.112
Fibrolamellar carcinoma	0 (0%)	3 (0.8%)	
Hepatocellular carcinoma	185 (49.5%)	179 (47.9%)	
Hepatocholangiocarcinoma (mixed)	2 (0.5%)	5 (1.3%)	
Histologic grade, n (%)			0.513
G1	28 (7.6%)	27 (7.3%)	
G2	95 (25.7%)	83 (22.5%)	
G3	56 (15.2%)	68 (18.4%)	
G4	7 (1.9%)	5 (1.4%)	

Table 1. Continued.

Characteristics	Low expression of CNTN6	High expression of CNTN6	*p*-value
AFP (ng/mL), n (%)			0.504
≤400	116 (41.4%)	99 (35.4%)	
>400	32 (11.4%)	33 (11.8%)	
Albumin(g/dL), n (%)			0.081
<3.5	42 (14%)	27 (9%)	
≥3.5	113 (37.7%)	118 (39.3%)	
Prothrombin time, n (%)			0.160
≤4	112 (37.7%)	96 (32.3%)	
>4	40 (13.5%)	49 (16.5%)	
Vascular invasion, n (%)			0.011
No	118 (37.1%)	90 (28.3%)	
Yes	46 (14.5%)	64 (20.1%)	
Adjacent hepatic tissue inflammation, n (%)			0.005
None	48 (20.3%)	70 (29.5%)	
Mild	55 (23.2%)	46 (19.4%)	
Severe	14 (5.9%)	4 (1.7%)	

LIHC, liver hepatocellular carcinoma; AFP, alpha-fetoprotein.

independent cohort for validation; the clinical expression pattern and prognostic value of CNTN6 were further validated via tissue microarray analysis of 92 paired tumor and paracancerous specimens, providing clinical support for subsequent *in vitro* and *in vivo* mechanistic investigations (**Supplementary Fig. 1A,B**). Immunohistochemical staining revealed distinct heterogeneity in CNTN6 expression between tumor and paracancerous tissues (Fig. 5A). All cases were categorized into three subgroups according to relative CNTN6 expression levels: tumor high-expression, equivalent expression, and tumor low-expression. Quantitative distribution analysis (Fig. 5B) demonstrated that 59.8% of patients exhibited higher CNTN6 expression in tumor tissues, 22.8% showed comparable expression between paired tissues, and 17.4% presented lower tumor CNTN6 expression. Clinicopathological correlation analysis indicated that CNTN6 expression was significantly upregulated in tumors with lymph node metastasis (Fig. 5C). CNTN6 expression levels differed significantly across TNM stages (Fig. 5D), with stage IV tumors exhibiting markedly higher CNTN6 abundance than stage II tumors. Patients were stratified into high- and low-CNTN6 expression groups based on the median cutoff value. Kaplan–Meier survival analysis revealed that elevated CNTN6 expression was significantly associated with OS ($p = 0.007$) and significantly impaired recurrence-free survival (RFS, $p = 0.005$) (Fig. 5E,F). Univariate Cox regression analysis was performed to assess the prognostic implications of CNTN6 expression and multiple clinicopathological variables, including sex, age, tumor differentiation, AFP level, lymph node metastasis, vascular invasion, tumor type, primary tumor number, and TNM stage. CNTN6 expression, lymph node metastasis status, and TNM stage were identified as significant prognostic factors ($p < 0.05$) (Fig. 5G).

3.6 CNTN6 Knockdown Represses Cell Proliferation, Migration, and Invasion While Inducing Apoptosis in HCC Cells in Vitro

To verify prior bioinformatic findings, we constructed stable CNTN6-knockdown MHCC-97H line by lentiviral *shCNTN6* transduction, with shNC serving as a negative control. WB results confirmed efficient CNTN6 protein downregulation (Fig. 6A,B). Comprehensive functional characterization of CNTN6 knockdown in HCC cell lines revealed consistent suppression of oncogenic phenotypes. Comparative analysis between shRNA-treated groups and scramble control (shNC) cohorts demonstrated markedly attenuated cellular proliferation, as shown by CCK-8 assay results (Fig. 6C). Furthermore, long-term clonogenic survival assays corroborated these findings, revealing significant diminution of colony-forming efficiency in CNTN6-deficient populations (Fig. 6D,E). Wound-healing assay results demonstrated that the CNTN6-low expression group exhibited significantly decreased tumor cell migration ability (Fig. 6F). Transwell assays showed that CNTN6 knockdown reduced both cell migratory and invasive capacities (Fig. 6G). EdU incorporation assays suggested that CNTN6-low expression affected the proliferation ability of tumor cells (Fig. 6H). Flow cytometry analysis indicated an increased apoptosis rate of tumor cells in the shRNA group (Fig. 6I). Taken together, these *in vitro* functional experiments demonstrated that CNTN6 depletion broadly restrained the tumorigenic traits of HCC cells, encompassing cell proliferation, colony formation, migration, and invasion, and simultaneously accelerated HCC cell apoptosis.

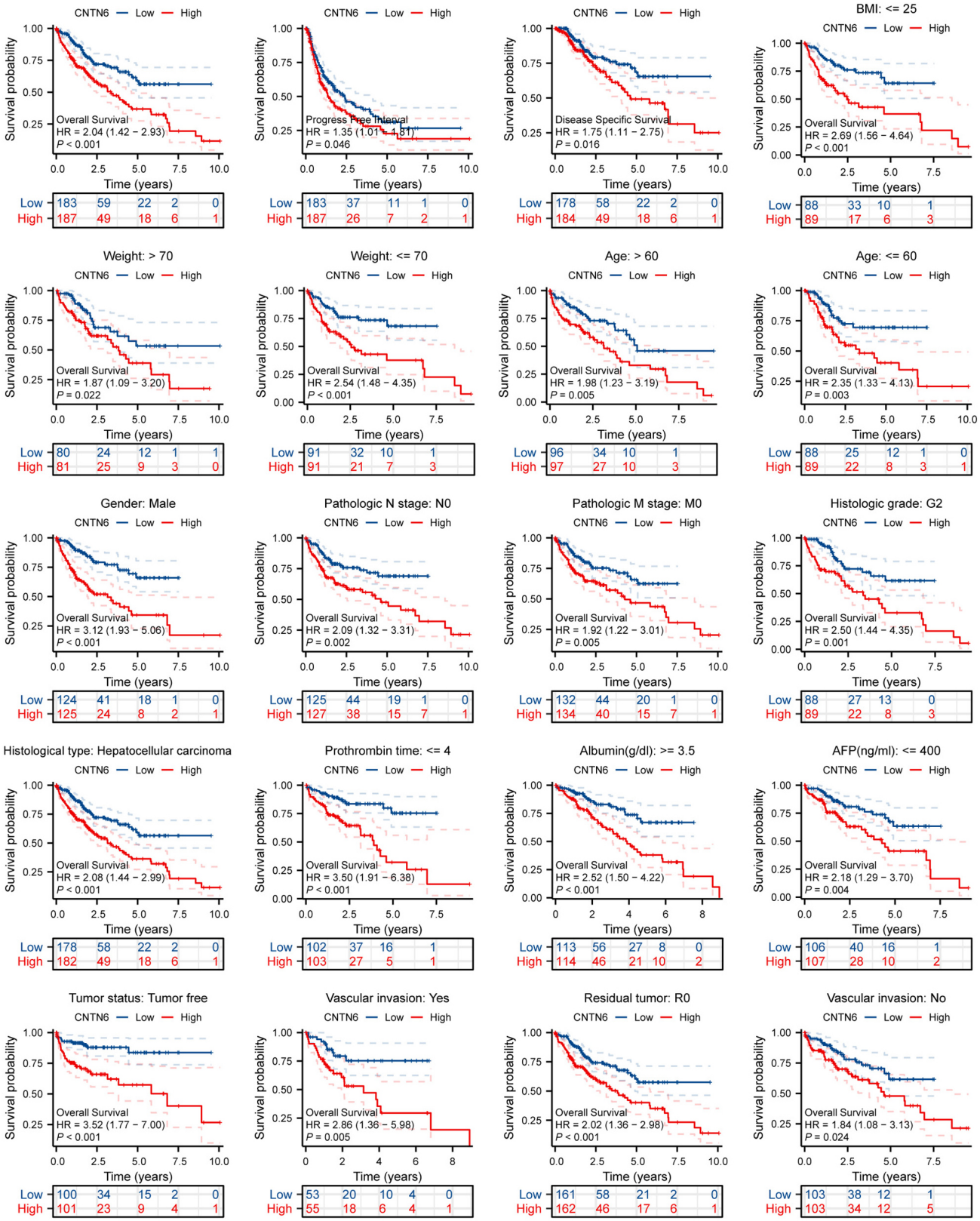


Fig. 2. Kaplan-Meier survival analyses according to CNTN6 expression in The Cancer Genome Atlas (TCGA)-LIHC and clinical subgroups. In cases of liver cancer, Kaplan-Meier curves showing overall survival (OS), disease-specific survival (DSS), and progression-free interval (PFI) according to high versus low CNTN6 expression in the overall cohort and indicated clinical subgroups are presented. Log-rank *p*-values are shown.

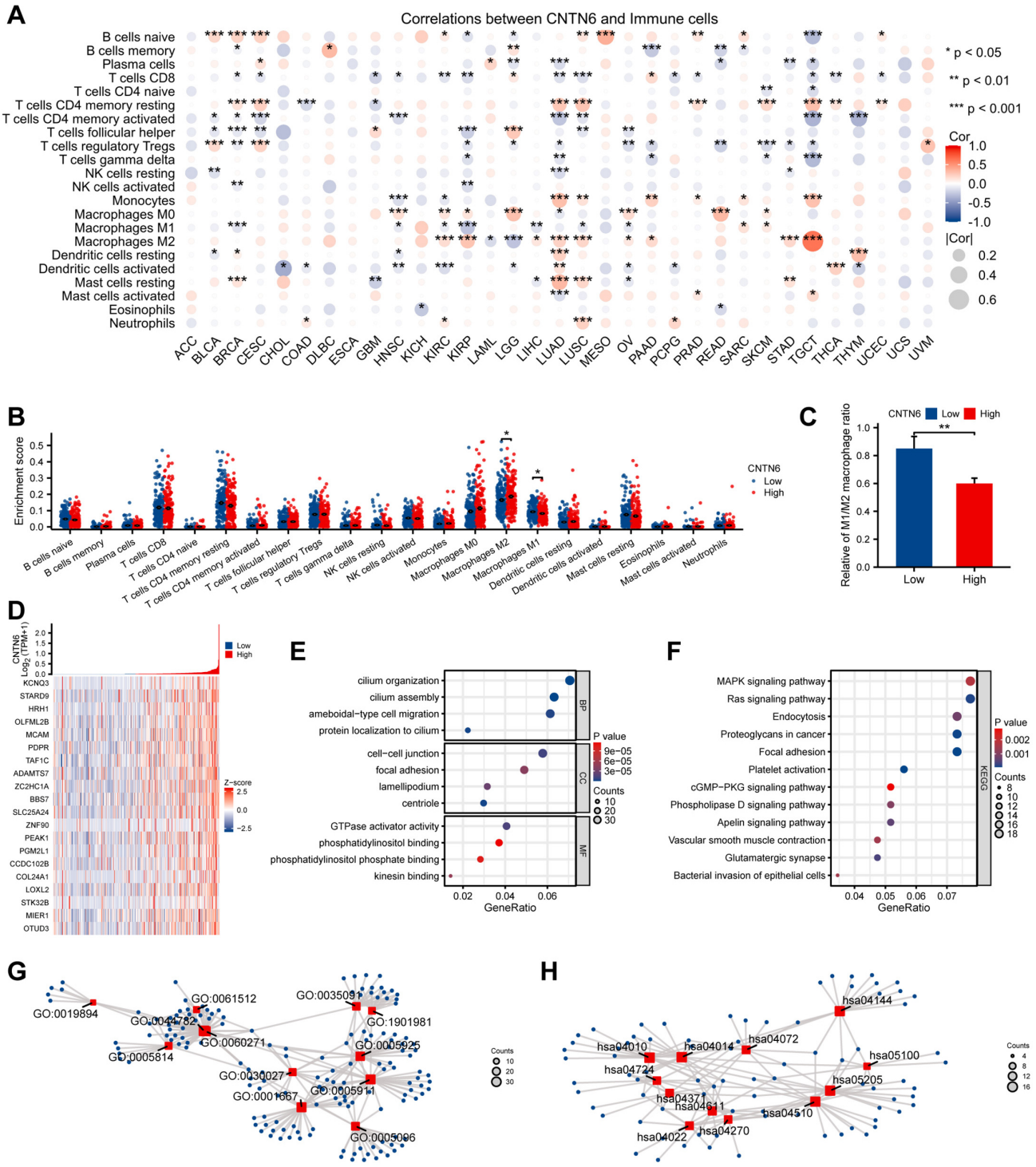


Fig. 3. Association of CNTN6 expression with immune cell infiltration and CNTN6-related functional networks. (A) In pan-cancer analysis, the association between CNTN6 and immune cells showed that the size and color of the circles (from blue to red) were proportional to the degree of association. (B) In the analysis of the correlation between CNTN6 and immune cells in HCC, CNTN6 expression was associated with M1- and M2-like macrophage infiltration estimates in LIHC. (C) The expression level of CNTN6 was related to the ratio of M1/M2. (D) Heatmap for the correlation analysis of CNTN6 with tumor-related molecules. (E,F) Kyoto Encyclopedia of Genes and Genomes (KEGG) and Gene Ontology (GO) analyses of CNTN6 were closely related to tumor progression and cell signaling-related molecular pathways. (G) GO enrichment network. Red squares represent enriched GO terms, and blue circles represent the genes involved in each term. (H) KEGG pathway enrichment network. Red squares represent enriched KEGG pathways, and blue circles represent the corresponding genes. Circle size is proportional to the gene count of each term. *$p < 0.05$; **$p < 0.01$; ***$p < 0.001$.

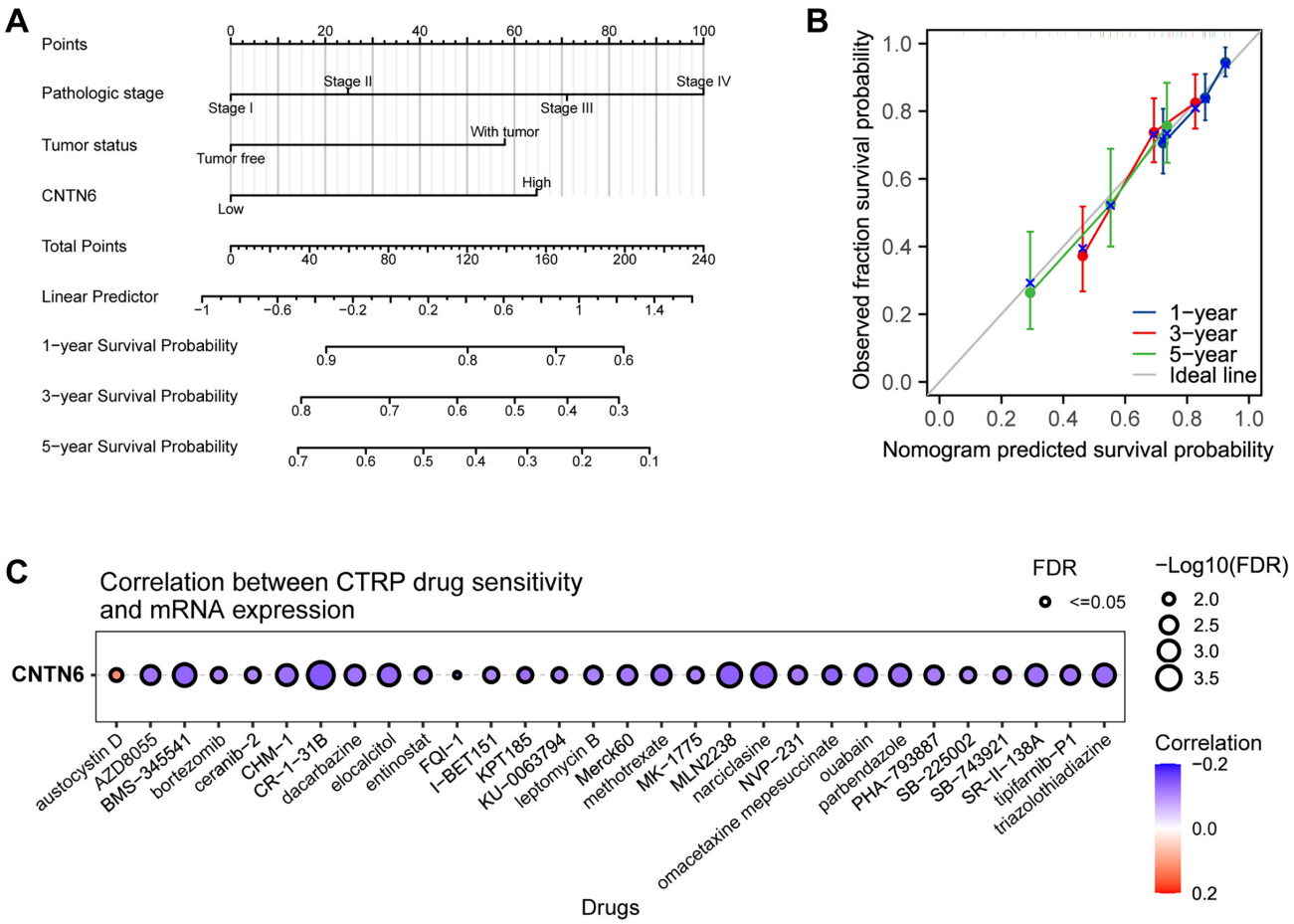


Fig. 4. CNTN6-related prognostic nomogram and Cancer Therapeutics Response Portal (CTRP) drug sensitivity correlation analysis in LIHC. (A) Nomogram for predicting 1-, 3-, and 5-year OS rates. (B) Calibration curve for the nomogram. (C) Correlation between CNTN6 expression and CTRP drug sensitivity scores.

3.7 CNTN6 Overexpression Facilitates HCC Cell Proliferation, Migration, and Invasion and Participates in Macrophage Polarization in Vitro

To further strengthen the core evidence for the oncogenic role of CNTN6 in HCC, we established stable CNTN6-overexpressing MHCC-97H cell line, with cells transduced with an empty vector serving as negative controls. Western blot analysis confirmed a significant upregulation of CNTN6 protein in CNTN6-overexpressing HCC cells, verifying the successful construction of stable overexpression cell lines (Fig. 7A,B). Subsequent functional rescue assays were performed to systematically validate the oncogenic phenotypes induced by CNTN6 upregulation. The CCK-8 assay demonstrated that CNTN6 overexpression markedly enhanced the proliferative capacity of MHCC-97H cells compared with the negative control group (Fig. 7C). Wound-healing assays showed that elevated CNTN6 expression significantly promoted the migratory capacity of HCC cells (Fig. 7D). Furthermore, Transwell migration and invasion assays confirmed that CNTN6 overexpression effectively strengthened the migratory and invasive potentials of HCC cells, firmly supporting the pro-tumorigenic and pro-metastatic effects of CNTN6 (Fig. 7E). To further explore the potential mechanism underlying the oncogenic function of CNTN6 beyond intrinsic tumor-cell phenotypes, we constructed a co-culture system of HCC cells and macrophages. Flow cytometry analysis revealed that CNTN6 overexpression significantly increased the proportion of M2-type polarized macrophages within the co-culture microenvironment (Fig. 7F). Consistently, significantly elevated concentrations of IL-10 and TGF-β were detected in the culture supernatants of the co-culture system (Fig. 7G). Collectively, these experiments demonstrated that CNTN6 facilitates malignant progression of HCC by promoting intrinsic tumor-cell proliferation, migration, and invasion, and concurrently driving macrophage polarization, thereby further consolidating the oncogenic role of CNTN6 in hepatocellular carcinoma.

3.8 CNTN6 Knockdown Suppresses Xenograft Tumor Growth in Vivo

Cell culture-based investigations established that CNTN6 depletion substantially curbed HCC cell proliferation, colony formation, and tumorigenic potential *in*

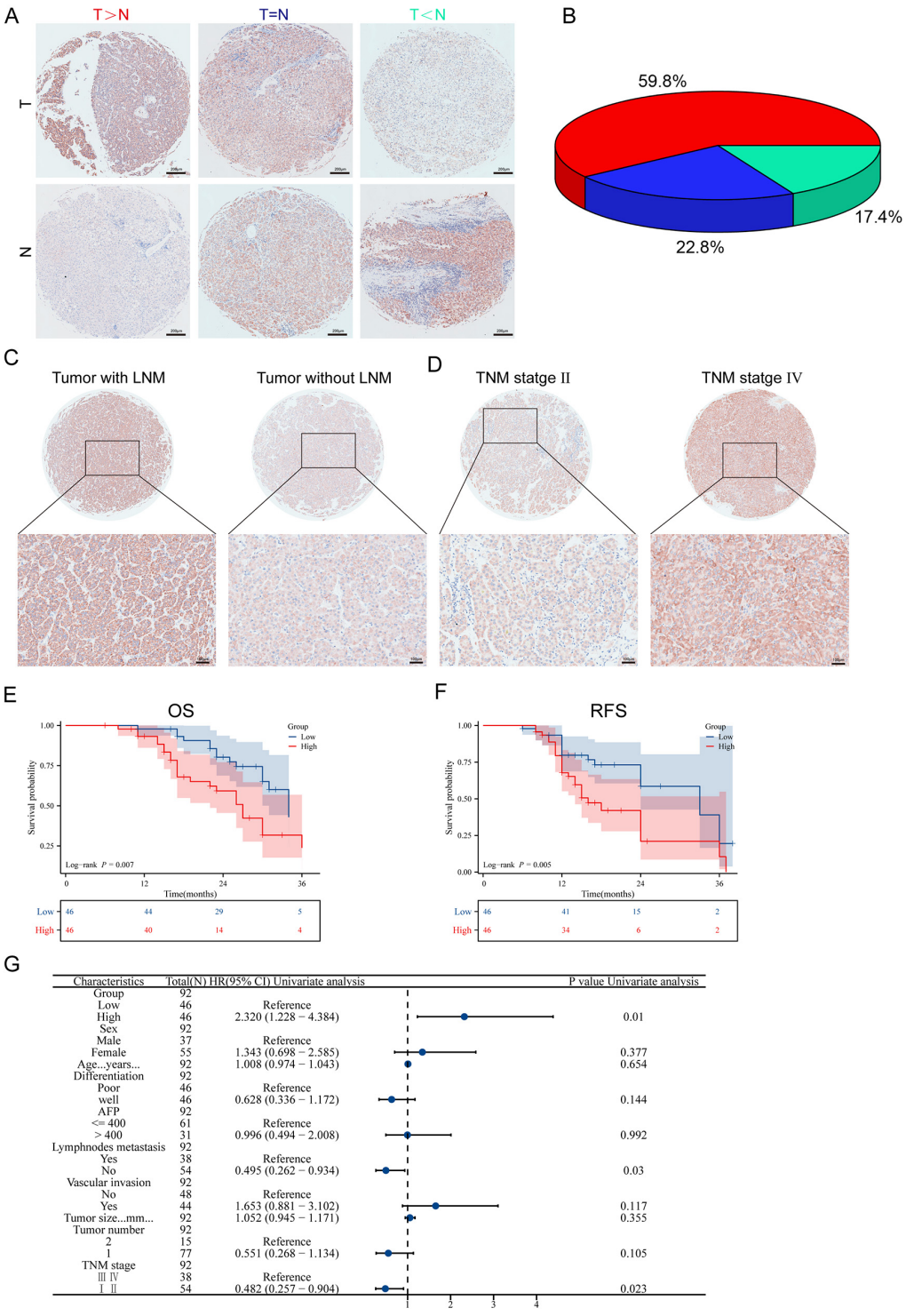


Fig. 5. Expression profiles and prognostic value of CNTN6 in human clinical tumor tissues. (A) Representative immunohistochemical images showing three distinct CNTN6 expression patterns in paired tumor and paracancerous tissues. Red indicates tumors with high CNTN6 expression, blue indicates consistent CNTN6 expression between tumor and paracancerous tissues, and green indicates tumors with low CNTN6 expression. The bar represents 200 μm. (B) Pie chart illustrating the proportional distribution of patients with the three CNTN6 expression subtypes, with red, blue, and green sectors corresponding to tumor high-expression, equivalent-expression, and low-expression subgroups, respectively. (C) Representative CNTN6 staining images of tumor tissues from patients with or without lymph node metastasis. The bar represents 100 μm. (D) Differential CNTN6 expression in tumor tissues between patients with Tumor–Node–Metastasis (TNM) stage II and stage IV disease. (E) Kaplan–Meier curves of OS stratified by CNTN6 expression levels. (F) Kaplan–Meier curves of recurrence-free survival (RFS) stratified by CNTN6 expression levels. (G) Forest plot of univariate Cox regression analysis for prognostic factors of patient survival.

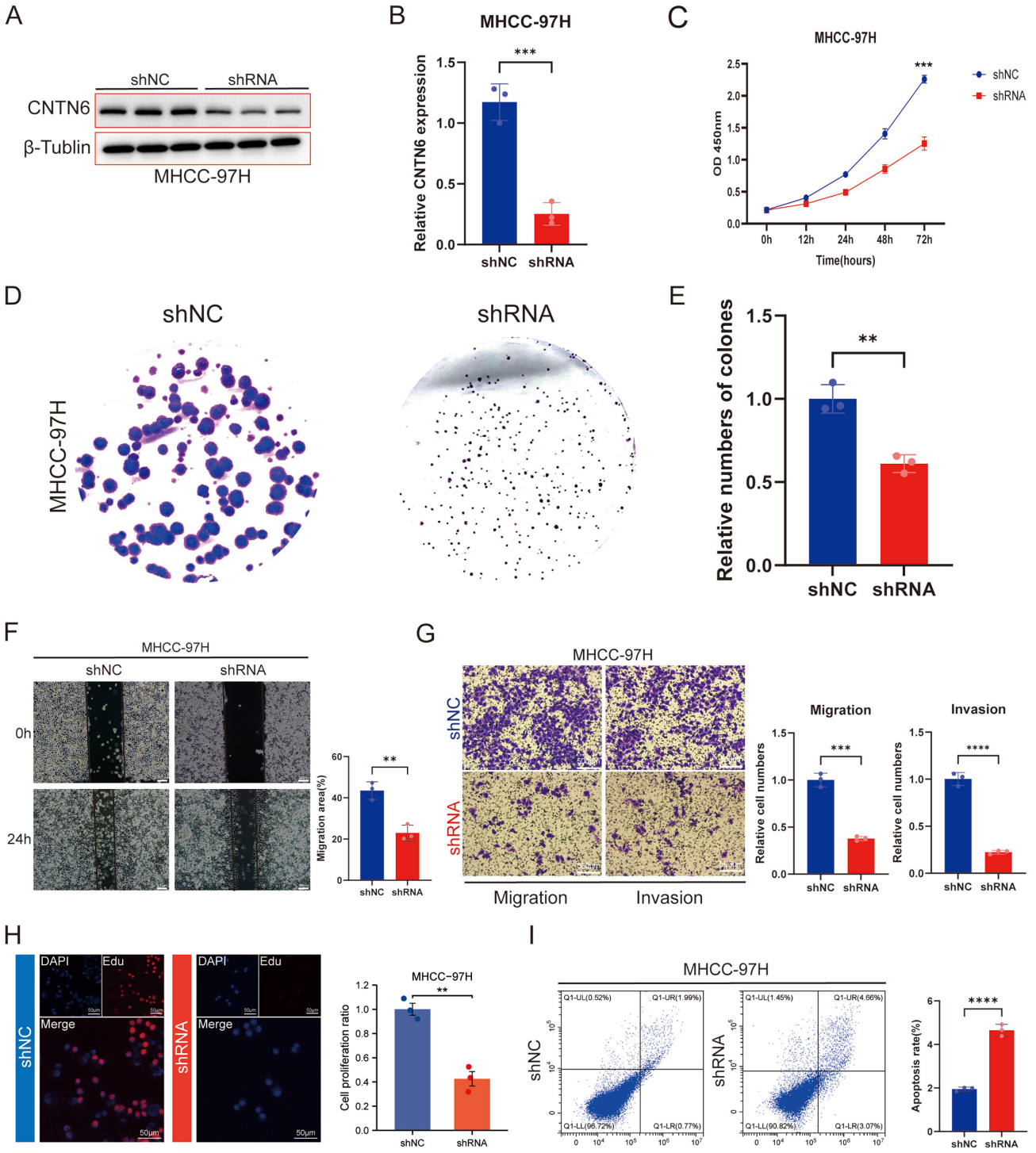


Fig. 6. CNTN6 knockdown suppresses HCC cell proliferation, migration, invasion, and colony formation *in vitro*. (A,B) Western blot (WB) analysis and quantification of CNTN6 knockdown efficiency in MHCC-97H cells. (C) Cell Counting Kit-8 (CCK-8) assay results. (D,E) Colony formation assays. (F) Wound-healing assay results. The bar represents 200 μm. (G) Transwell invasion and migration assay findings. (H) EdU incorporation assay observations. The bar represents 50 μm. (I) Flow cytometric analysis of cell apoptosis. $^{**}p < 0.01$; $^{***}p < 0.001$; $^{****}p < 0.0001$.

vitro. Therefore, we conducted experiments in mice (Fig. 8A). MHCC-97H cells stably expressing shNC or *shCNTN6* were subcutaneously inoculated into BALB/c nude mice. Fourteen days after inoculation, tumors were excised, photographed, and weighed, and tumor volumes were calculated from caliper measurements. The results showed that tumor sizes and weights in the *shCNTN6* group were lower than those in the shNC group (Fig. 8B–F). Histo-

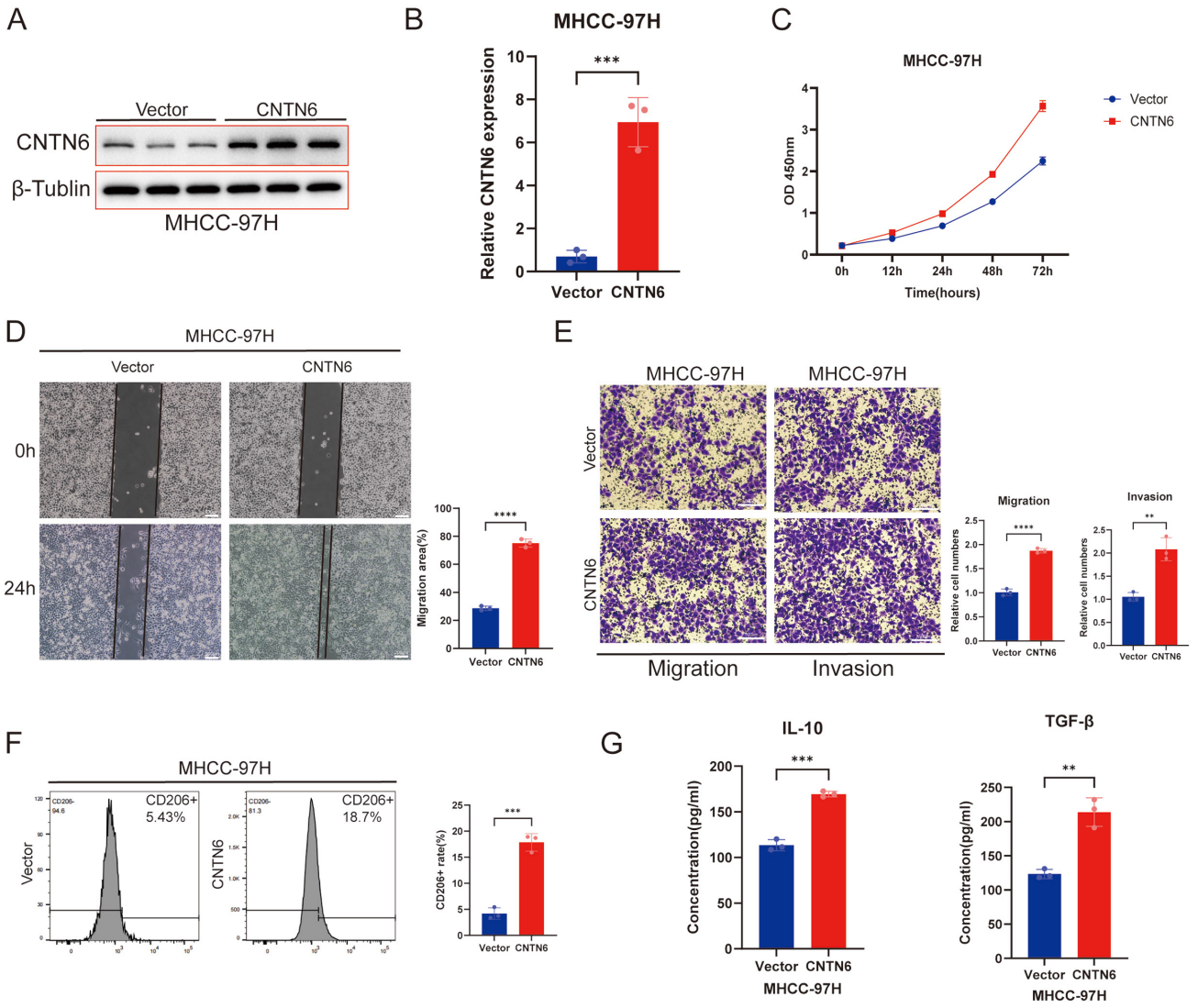


Fig. 7. CNTN6 overexpression facilitates HCC cell proliferation, migration, and invasion and participates in macrophage polarization *in vitro*. (A,B) Western blot analysis and quantification of CNTN6 overexpression efficiency in MHCC-97H cells. (C) CCK-8 assays. (D) Wound healing assay. The bar represents 200 μm. (E) Transwell invasion and migration assays. The bar represents 500 μm. (F) Flow cytometry analysis of M2-like macrophage proportion in co-culture system. (G) Expression of interleukin-10 (IL-10) and transforming growth factor-β (TGF-β) was detected using ELISA after co-culture with HCC cells. $^{**}p < 0.01$; $^{***}p < 0.001$; $^{****}p < 0.0001$.

logical and immunostaining analyses of xenograft tumors further supported the inhibitory effect of CNTN6 knockdown on tumor growth (Fig. 8G–I). Meanwhile, we conducted double fluorescence staining analysis for CD86 and CD206 markers and displayed the results using 3D visualization. Immunofluorescence staining revealed increased CD86 signals and decreased CD206 signals in *shCNTN6* tumors compared with shNC tumors (Fig. 8J). These findings suggest that CNTN6 knockdown was associated with a shift from CD206-dominant to CD86-dominant immune staining in xenograft tumors, implying a potential relationship between CNTN6 and macrophage-associated immune remodeling.

4. Discussion

HCC is a highly heterogeneous and "immune-cold" malignancy with poor patient prognosis [42], and identification of robust prognostic biomarkers and immune-related oncogenic drivers is urgently needed. CNTN6 is a cell adhesion molecule of the immunoglobulin superfamily, but its role in HCC has not been systematically defined. In the present study, we provide comprehensive evidence that *CNTN6* is upregulated in HCC, predicts poor survival, promotes malignant phenotypes *in vitro* and *in vivo*, and participates in the remodeling of the hepatocellular carcinoma tumor immune microenvironment by promoting M2 macrophage polarization and increasing the secretion of

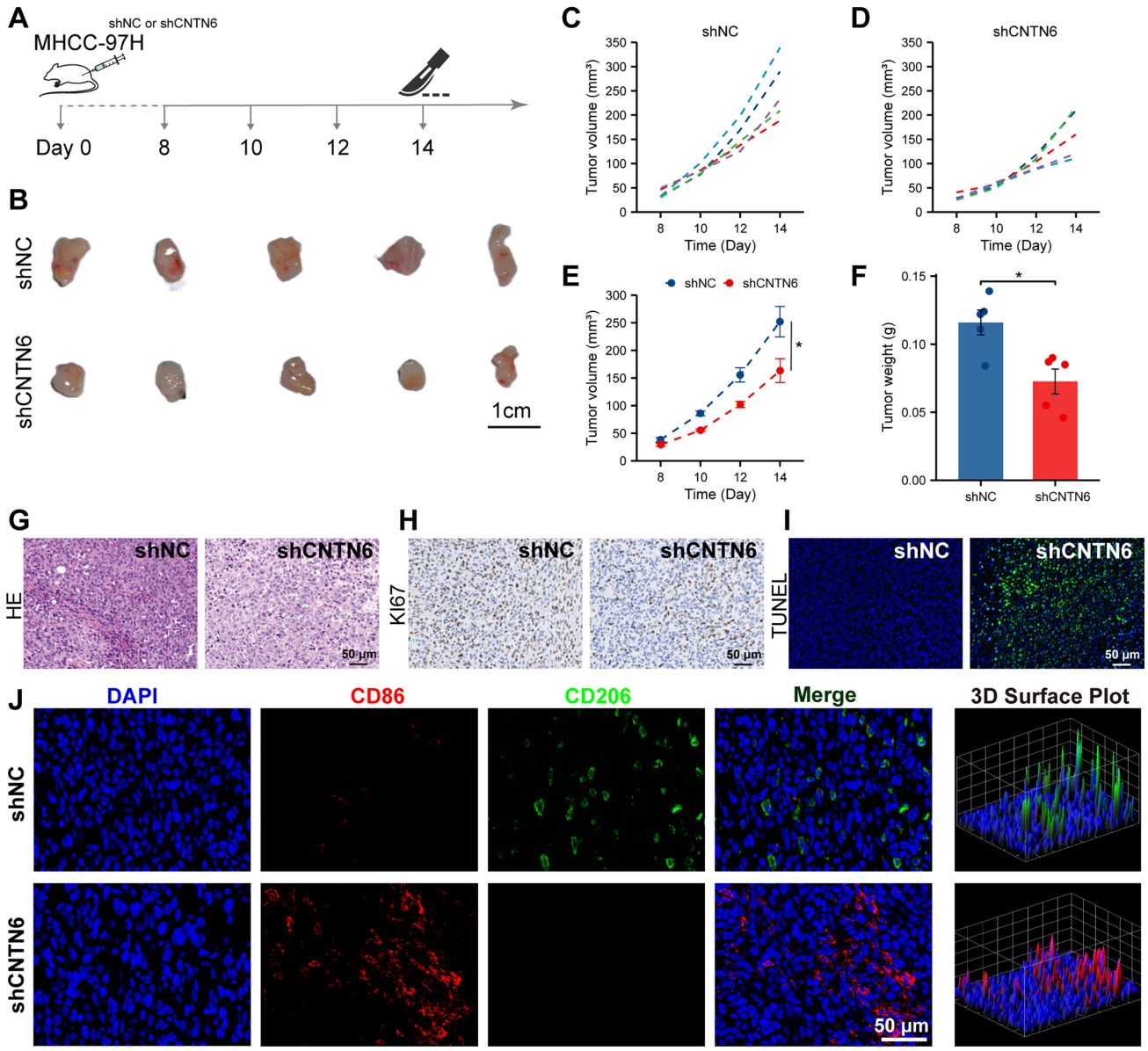


Fig. 8. CNTN6 knockdown inhibits xenograft tumor growth and alters CD86/CD206 staining *in vivo*. (A) Workflow diagram of animal experiments. BALB/c nude mice were subcutaneously inoculated with MHCC-97H cells stably expressing shNC or *shCNTN6*. After 14 days, the tumors were harvested. (B) Visual images of mouse tumors. (C–I) Statistical analyses of volumes and weights of tumors from the two groups, and Immunohistochemical staining of mouse tumors. Scale bar: 50 μm. (J) Representative immunofluorescence staining of 4′,6-diamidino-2-phenylindole (DAPI) (blue), CD86 (red), and CD206 (green), together with 3D surface plots. Scale bar: 50 μm. *$p < 0.05$.

immunosuppressive cytokines (IL-10 and TGF-β). These findings identify *CNTN6* as a novel tumor promoter and a promising prognostic and immune-related biomarker in HCC [4].

Consistent with cancer-associated dysregulation of cell adhesion molecules, our data from TCGA, GTEx, and HPA consistently demonstrated that *CNTN6* was significantly elevated in HCC tissues compared with normal liver tissues at both the mRNA and protein levels. High *CNTN6* expression was associated with multiple clinicopathological features, including pathologic N stage and adjacent hepatic inflammation, supporting its potential involvement in HCC progression [7]. These results expand the expression spectrum of *CNTN6* beyond neural tissues and establish it as a dysregulated molecule in liver cancer.

Survival analysis further revealed that high *CNTN6* expression was significantly associated with shorter OS, PFI, and DSS in HCC patients [8]. Stratified analyses confirmed its stable prognostic value across multiple clinical subgroups, supporting its potential as an independent prognostic indicator. Meanwhile, we conducted a KM curve analysis by combining the prognosis information of

92 HCC patients in our center with the expression levels of CNTN6, which indicated that high *CNTN6* expression was negatively correlated with prognosis. To improve clinical practicability, we constructed a prognostic nomogram incorporating *CNTN6* expression, pathologic stage, and tumor status, which revealed favorable predictive performance for 1-, 3-, and 5-year OS. Collectively, these data support that *CNTN6* can serve as a reliable prognostic stratification marker for HCC patients.

A key finding of this study is the link between *CNTN6* and macrophage-mediated immune remodeling. Immune-cell infiltration analysis revealed a positive correlation between *CNTN6* and M2-like macrophage infiltration in HCC [36]. *In vitro* Transwell non-contact coculture and flow cytometry-based assays further corroborated that high *CNTN6* expression in HCC cells promotes M2 macrophage polarization, suggesting that *CNTN6* may contribute to reshaping the HCC immune microenvironment via modulating macrophage phenotypes. Moreover, *CNTN6* was associated with M2 markers and immunosuppressive molecules. *In vivo* xenograft models further confirmed that CNTN6 knockdown increased CD86 (M1) and decreased CD206 (M2) staining, indicating a shift from a pro-tumor M2 to an anti-tumor M1 phenotype. The *in vitro* cell co-culture experiments revealed that overexpression of *CNTN6* promoted the secretion of immune-suppressive cytokines such as IL-10 and TGF-β. These results suggest that *CNTN6* may shape an immunosuppressive microenvironment by regulating macrophage polarization and increasing immunosuppressive cytokines [32], which represents a non-cell-autonomous mechanism underlying HCC progression [33].

Functional experiments validated the oncogenic role of *CNTN6* in HCC. *In vitro*, knockdown of *CNTN6* significantly inhibited proliferation, colony formation, migration, and invasion by MHCC-97H cells, and Overexpression of *CNTN6* enhanced the malignant phenotype of tumor cells. *In vivo*, silencing *CNTN6* markedly suppressed xenograft tumor growth [43]. Functional enrichment indicated that CNTN6-related genes were enriched in cell migration and oncogenic signaling pathways, consistent with the pro-tumor function of *CNTN6*. These results demonstrated that *CNTN6* acts as a tumor-promoting agent in HCC by sustaining cell growth and metastatic potential.

Drug sensitivity analysis based on CTRP revealed that *CNTN6* expression was negatively correlated with sensitivity to multiple compounds, including BMS-345541, MLN2238, and ouabain. This suggests that CNTN6 may be associated with therapeutic responses and that patients with low *CNTN6* expression might derive greater benefit from certain agents. The CCK8 experiment demonstrated that MLN2238 had a significant inhibitory effect on the viability of liver cancer cells that overexpressed *CNTN6*. These observations provide preliminary clues for precision therapy, although further experimental validation is required.

5. Limitations

Our study has several limitations. First, *in vivo* xenograft experiments were performed in T-cell-deficient nude mice, which fail to recapitulate the intact immune microenvironment of clinical HCC, thus restricting the interpretation of immune-related findings. Second, upstream epigenetic and miRNA regulatory analyses of CNTN6 relied solely on bioinformatic predictions from public datasets without experimental validation. Furthermore, the identified macrophage-associated miRNAs likely mediate indirect crosstalk within the tumor microenvironment rather than directly modulating CNTN6. Finally, we focused only on the oncogenic and prognostic roles of CNTN6 in HCC, while potential compensatory or off-target effects following CNTN6 inhibition remain uncharacterized. Further mechanistic validation is warranted to delineate the precise CNTN6 regulatory network in HCC.

6. Conclusions

In summary, the present study demonstrated that *CNTN6* is aberrantly upregulated in HCC and serves as a pivotal oncogenic regulator that promotes malignant progression and predicts adverse clinical outcomes. Functional validation confirmed the pro-tumor role of *CNTN6* in HCC and its capacity to modulate macrophage polarization and reshape the tumor immune microenvironment. Collectively, our results identify *CNTN6* as a reliable prognostic biomarker and a potential therapeutic target for HCC, offering novel mechanistic insights into immune-related oncogenesis of liver cancer.

Availability of Data and Materials

Data are available from the corresponding author upon reasonable request.

Author Contributions

RY: Conceptualization, Data curation, Formal analysis, Writing - original draft. JY: Investigation, Methodology. JZ: Resources, Validation, Formal analysis. YP: Resources, Data curation. WG: Methodology, Investigation. CY: Conception and design, Supervision, Funding acquisition, Writing - review and editing. All authors contributed to editorial changes in the manuscript. All authors read and approved the final manuscript. All authors have participated sufficiently in the work and agreed to be accountable for all aspects of the work.

Ethics Approval and Consent to Participate

The TMA approval process was reviewed by the Medical Ethics Committee of Hunan Provincial People's Hospital/The First Affiliated Hospital of Hunan Normal University (IRB Approval No.: 2024-302). Informed consent was obtained from the patients, and personally identifiable information was processed for all samples. The study was

carried out in accordance with the guidelines of the Declaration of Helsinki. The animal study protocol was approved by the Animal Ethics Committee of Hunan Provincial People's Hospital/The First Affiliated Hospital of Hunan Normal University (approval no. 2025062). All animal experiments were approved by the Animal Ethics Committee of Hunan Provincial People's Hospital/The First Affiliated Hospital of Hunan Normal University. All animal experimental procedures were performed in accordance with the guidelines of this committee and complied with the 3Rs principles (Replacement, Reduction, Refinement). This study was reported following the ARRIVE guidelines for animal research, and animal welfare was implemented in strict accordance with the requirements of the Animal Ethics Committee of Hunan Provincial People's Hospital/The First Affiliated Hospital of Hunan Normal University.

Acknowledgment

Not applicable.

Funding

This work was supported by the National Natural Science Foundation of China (grant no. 82373293), the Jiangsu Commission of Health (grant no. ZD2022063), and the Jiangsu Province Graduate Student Practice and Innovation Program (grant no. SJCX25_0823).

Conflicts of Interest

The authors declare no conflicts of interest.

Supplementary Material

Supplementary material associated with this article can be found, in the online version, at https://doi.org/10.31083/FBL55597.

References

[1] Sung H, Ferlay J, Siegel RL, Laversanne M, Soerjomataram I, Jemal A, et al. Global Cancer Statistics 2020: GLOBOCAN Estimates of Incidence and Mortality Worldwide for 36 Cancers in 185 Countries. CA: a Cancer Journal for Clinicians. 2021; 71: 209–249. https://doi.org/10.3322/caac.21660

[2] Zou Y, Wan X, Zhou Q, Zhu G, Lin S, Tang Q, et al. Mechanisms of drug resistance in hepatocellular carcinoma. Biological Procedures Online. 2025; 27: 19. https://doi.org/10.1186/s12575-025-00281-6

[3] Zhang Z, Chen B, Liu Y, Zhang K, Wei Z, Dai Y, et al. Advances in Nanomedicine for Targeting Cancer Stem Cells and Overcoming Therapeutic Resistance. ACS Nano. 2025; 19: 30720–30757. https://doi.org/10.1021/acsnano.5c02321

[4] Llovet JM, Pinyol R, Kelley RK, El-Khoueiry A, Reeves HL, Wang XW, et al. Molecular pathogenesis and systemic therapies for hepatocellular carcinoma. Nature Cancer. 2022; 3: 386–401. https://doi.org/10.1038/s43018-022-00357-2

[5] Llovet JM, Kelley RK, Villanueva A, Singal AG, Pikarsky E, Roayaie S, et al. Hepatocellular carcinoma. Nature Reviews. Disease Primers. 2021; 7: 6. https://doi.org/10.1038/s41572-020-00240-3

[6] Llovet JM, Pinyol R, Affo S, Yarchoan M, Gores GJ, Kelley RK, et al. Hallmarks of liver cancer: Therapeutic implications. Cell. 2026; 189: 2490–2514. https://doi.org/10.1016/j.cell.2026.03.001

[7] Craig AJ, von Felden J, Garcia-Lezana T, Sarcognato S, Villanueva A. Tumour evolution in hepatocellular carcinoma. Nature Reviews. Gastroenterology & Hepatology. 2020; 17: 139–152. https://doi.org/10.1038/s41575-019-0229-4

[8] Llovet JM, Montal R, Sia D, Finn RS. Molecular therapies and precision medicine for hepatocellular carcinoma. Nature Reviews. Clinical Oncology. 2018; 15: 599–616. https://doi.org/10.1038/s41571-018-0073-4

[9] Hamidi H, Ivaska J. Every step of the way: integrins in cancer progression and metastasis. Nature Reviews. Cancer. 2018; 18: 533–548. https://doi.org/10.1038/s41568-018-0038-z

[10] Janiszewska M, Primi MC, Izard T. Cell adhesion in cancer: Beyond the migration of single cells. The Journal of Biological Chemistry. 2020; 295: 2495–2505. https://doi.org/10.1074/jbc.REV119.007759

[11] Das J, Barman B, Sarma P, Das BK, Chetia R, Kalita PP. Signalling pathways in hepatocellular carcinoma (HCC) metastasis and invasion: Molecular mechanisms and therapeutic implications. Biochemistry and Biophysics Reports. 2025; 45: 102403. https://doi.org/10.1016/j.bbrep.2025.102403

[12] Shimoda Y, Watanabe K. Contactins: emerging key roles in the development and function of the nervous system. Cell Adhesion & Migration. 2009; 3: 64–70. https://doi.org/10.4161/cam.3.1.7764

[13] Zuko A, Kleijer KTE, Oguro-Ando A, Kas MJH, van Daalen E, van der Zwaag B, et al. Contactins in the neurobiology of autism. European Journal of Pharmacology. 2013; 719: 63–74. https://doi.org/10.1016/j.ejphar.2013.07.016

[14] Poot M. Intragenic *CNTNAP2* Deletions: A Bridge Too Far? Molecular Syndromology. 2017; 8: 118–130. https://doi.org/10.1159/000456021

[15] Chatterjee M, Schild D, Teunissen CE. Contactins in the central nervous system: role in health and disease. Neural Regeneration Research. 2019; 14: 206–216. https://doi.org/10.4103/1673-5374.244776

[16] Ringelhan M, Pfister D, O'Connor T, Pikarsky E, Heikenwalder M. The immunology of hepatocellular carcinoma. Nature Immunology. 2018; 19: 222–232. https://doi.org/10.1038/s41590-018-0044-z

[17] Binnewies M, Roberts EW, Kersten K, Chan V, Fearon DF, Merad M, et al. Understanding the tumor immune microenvironment (TIME) for effective therapy. Nature Medicine. 2018; 24: 541–550. https://doi.org/10.1038/s41591-018-0014-x

[18] Zhang Q, He Y, Luo N, Patel SJ, Han Y, Gao R, et al. Landscape and Dynamics of Single Immune Cells in Hepatocellular Carcinoma. Cell. 2019; 179: 829–845.e20. https://doi.org/10.1016/j.cell.2019.10.003

[19] Sun Y, Wu L, Zhong Y, Zhou K, Hou Y, Wang Z, et al. Single-cell landscape of the ecosystem in early-relapse hepatocellular carcinoma. Cell. 2021; 184: 404–421.e16. https://doi.org/10.1016/j.cell.2020.11.041

[20] Kole C, Charalampakis N, Tsakatikas S, Vailas M, Moris D, Gkotsis E, et al. Immunotherapy for Hepatocellular Carcinoma: A 2021 Update. Cancers. 2020; 12: 2859. https://doi.org/10.3390/cancers12102859

[21] Melero I, Yau T, Kang YK, Kim TY, Santoro A, Sangro B, et al. Nivolumab plus ipilimumab combination therapy in patients with advanced hepatocellular carcinoma previously treated with sorafenib: 5-year results from CheckMate 040. Annals of Oncology: Official Journal of the European Society for Medical Oncology. 2024; 35: 537–548. https://doi.org/10.1016/j.annonc.2024.03.005

[22] Tomczak K, Czerwińska P, Wiznerowicz M. The Cancer Genome Atlas (TCGA): an immeasurable source of knowledge. Contemporary Oncology (Poznan, Poland). 2015; 19: A68–A77. https://doi.org/10.5114/wo.2014.47136

[23] GTEx Consortium. The GTEx Consortium atlas of genetic regulatory effects across human tissues. Science (New York, N.Y.). 2020; 369: 1318–1330. https://doi.org/10.1126/science.aaz1776

[24] Thul PJ, Åkesson L, Wiking M, Mahdessian D, Geladaki A, Ait Blal H, et al. A subcellular map of the human proteome. Science (New York, N.Y.). 2017; 356: eaal3321. https://doi.org/10.1126/science.aal3321

[25] Chen B, Khodadoust MS, Liu CL, Newman AM, Alizadeh AA. Profiling Tumor Infiltrating Immune Cells with CIBERSORT. Methods in Molecular Biology (Clifton, N.J.). 2018; 1711: 243–259. https://doi.org/10.1007/978-1-4939-7493-1_12

[26] Yu G, Wang LG, Han Y, He QY. clusterProfiler: an R package for comparing biological themes among gene clusters. Omics: a Journal of Integrative Biology. 2012; 16: 284–287. https://doi.org/10.1089/omi.2011.0118

[27] Szklarczyk D, Kirsch R, Koutrouli M, Nastou K, Mehryary F, Hachilif R, et al. The STRING database in 2023: protein-protein association networks and functional enrichment analyses for any sequenced genome of interest. Nucleic Acids Research. 2023; 51: D638–D646. https://doi.org/10.1093/nar/gkac1000

[28] Warde-Farley D, Donaldson SL, Comes O, Zuberi K, Badrawi R, Chao P, et al. The GeneMANIA prediction server: biological network integration for gene prioritization and predicting gene function. Nucleic Acids Research. 2010; 38: W214–W220. https://doi.org/10.1093/nar/gkq537

[29] Baumann AA, Wolkenhauer O, Wolfien M. TCGADownloadHelper: simplifying TCGA data extraction and preprocessing. Frontiers in Genetics. 2025; 16: 1569290. https://doi.org/10.3389/fgene.2025.1569290

[30] Hou L, Xiong X, Park Y, Boix C, James B, Sun N, et al. Multitissue H3K27ac profiling of GTEx samples links epigenomic variation to disease. Nature Genetics. 2023; 55: 1665–1676. https://doi.org/10.1038/s41588-023-01509-5

[31] Sangro B, Sarobe P, Hervás-Stubbs S, Melero I. Advances in immunotherapy for hepatocellular carcinoma. Nature Reviews. Gastroenterology & Hepatology. 2021; 18: 525–543. https://doi.org/10.1038/s41575-021-00438-0

[32] Yang R, Lu C, Jian Q, Song Y, Sun B, He W, et al. HBV-driven expansion of CXCR6^{+}-exhausted T cells and CXCL16^{+} macrophage interaction: Implications for immunotherapy in HCC. Innovation (Cambridge (Mass.)). 2026; 7: 101274. https://doi.org/10.1016/j.xinn.2026.101274

[33] Mantovani A, Marchesi F, Malesci A, Laghi L, Allavena P. Tumour-associated macrophages as treatment targets in oncology. Nature Reviews. Clinical Oncology. 2017; 14: 399–416. https://doi.org/10.1038/nrclinonc.2016.217

[34] Mantovani A, Sica A, Allavena P, Garlanda C, Locati M. Tumor-associated macrophages and the related myeloid-derived suppressor cells as a paradigm of the diversity of macrophage activation. Human Immunology. 2009; 70: 325–330. https://doi.org/10.1016/j.humimm.2009.02.008

[35] Qian BZ, Pollard JW. Macrophage diversity enhances tumor progression and metastasis. Cell. 2010; 141: 39–51. https://doi.org/10.1016/j.cell.2010.03.014

[36] Cassetta L, Pollard JW. Targeting macrophages: therapeutic approaches in cancer. Nature Reviews. Drug Discovery. 2018; 17: 887–904. https://doi.org/10.1038/nrd.2018.169

[37] Ngambenjawong C, Gustafson HH, Pun SH. Progress in tumor-associated macrophage (TAM)-targeted therapeutics. Advanced Drug Delivery Reviews. 2017; 114: 206–221. https://doi.org/10.1016/j.addr.2017.04.010

[38] Iasonos A, Schrag D, Raj GV, Panageas KS. How to build and interpret a nomogram for cancer prognosis. Journal of Clinical Oncology: Official Journal of the American Society of Clinical Oncology. 2008; 26: 1364–1370. https://doi.org/10.1200/JCO.2007.12.9791

[39] Tan Z, Chen Y, Peng Y, Tang Y, Sun B, Zhou J, et al. Integration of Meta-Analysis and Network Pharmacology to Investigate the Pharmacological Mechanisms of Quercetin on Hepatocellular Carcinoma. Frontiers in Bioscience (Landmark Edition). 2025; 30: 46289. https://doi.org/10.31083/FBL46289

[40] Basu A, Bodycombe NE, Cheah JH, Price EV, Liu K, Schaefer GI, et al. An interactive resource to identify cancer genetic and lineage dependencies targeted by small molecules. Cell. 2013; 154: 1151–1161. https://doi.org/10.1016/j.cell.2013.08.003

[41] Rees MG, Seashore-Ludlow B, Cheah JH, Adams DJ, Price EV, Gill S, et al. Correlating chemical sensitivity and basal gene expression reveals mechanism of action. Nature Chemical Biology. 2016; 12: 109–116. https://doi.org/10.1038/nchembio.1986

[42] Reig M, Forner A, Rimola J, Ferrer-Fàbrega J, Burrel M, Garcia-Criado Á, et al. BCLC strategy for prognosis prediction and treatment recommendation: The 2022 update. Journal of Hepatology. 2022; 76: 681–693. https://doi.org/10.1016/j.jhep.2021.11.018

[43] Hanahan D, Weinberg RA. Hallmarks of cancer: the next generation. Cell. 2011; 144: 646–674. https://doi.org/10.1016/j.cell.2011.02.013